Electric Power Systems Research 262 (2027) 113579



Contents lists available at ScienceDirect

Electric Power Systems Research

journal homepage: www.elsevier.com/locate/epsr





Optimal scheduling of flexible resources under uncertainty in multi-energy systems ⋆

Muyang Li [a,*], Sai Pavan Polisetty [b,1], Bikash C. Pal [b,2]

[a] School of Engineering, University of Warwick, Coventry, United Kingdom
[b] Department of Electrical and Electronics Engineering, Imperial College London, London, United Kingdom

ARTICLE INFO

Keywords:
Integrated energy systems
Two-stage robust optimization
Electric vehicles
Wind generation uncertainty
Mixed-integer linear programming (MILP)

ABSTRACT

With the increasing penetration of renewable energy and the rising demand for decarbonization, multi-energy systems integrating electricity, heat, and transportation sectors have attracted significant attention. However, the intermittency and uncertainty of renewable generation in integrated energy systems (IES) makes it difficult to ensure cost-effective and coordinated operation across different energy carriers, often leading to suboptimal use of system flexibility and increased operational risk. This paper proposes a robust optimization framework for integrated electric and thermal energy systems with vehicle-to-grid (V2G) enabled electric vehicles. This approach employs a linearized model for the distribution network and a constant flow variable temperature (CFVT) methodology for the heating system to balance accuracy and computational tractability. A two-stage formulation captures day-ahead EV charging commitments and real-time adaptive dispatch against wind generation uncertainty. An exact column-and-constraint generation algorithm ensures solution scalability and worst-case feasibility. Simulations on an IEEE 15-bus network and a 5-node district heating system illustrate the cost–robustness trade-off achieved by leveraging EV and thermal flexibility under the proposed robust scheduling approach, compared with stochastic scheduling.

1. Introduction

Driven by the net-zero carbon target, the installed capacity and generation share of renewable energy sources (RES) in the UK have continued to increase rapidly. The 2024 statistics show that the share of electricity generated from renewables exceeded 50% for the first time, reaching 50.8% compared to 46.4% in 2023 [1], reflecting the increasing role of wind power in the electricity system. However, the rapid deployment of renewable generation also introduces new operational challenges for power systems. The rapid growth of RES has outpaced grid expansion, causing energy spillage and high compensation costs [2]. Expanding transmission can reduce curtailment but is costly and slow [3]. Alternatively, flexible electrical storage (FES) improves system flexibility and resilience by balancing generation and demand [4].

Electric vehicles (EVs) with vehicle-to-grid (V2G) capability constitute a cost-effective form of flexible electrical storage (FES) and can provide distributed flexibility to support power system operation [5]. In addition to electrical flexibility, the heating sector also plays a significant role in energy system decarbonization and renewable energy utilization. Heating accounts for nearly 50% of global final energy consumption [6]. Electrifying heating or using renewable electricity for heat production is recognized as a key pathway to improve RES utilization and reduce carbon emissions [7]. Integrated energy systems (IES) have emerged as an effective approach to increase renewable integration and system flexibility by introducing multiple energy carriers on the supply side (e.g., wind, solar, natural gas), coordinating electric and thermal demands on the load side, and leveraging storage resources.

Meanwhile, the increasing penetration of renewable energy also introduces significant operational uncertainty for such integrated systems. High renewable variability and forecasting challenges remain key barriers to reliable and economic scheduling. Traditional deterministic dispatch relies on point forecasts and may lead to operational infeasibility when renewable output deviates from predictions. To address this issue, uncertainty-aware optimization methods have been widely studied, including stochastic optimization (SO) and robust optimization (RO). SO captures uncertainty through probability distributions [8,9], while RO

⋆ Submitted to the 24th Power Systems Computation Conference (PSCC 2026).

* Corresponding author.
E-mail addresses: muyang.li.2@warwick.ac.uk (M. Li), s.polisetty@imperial.ac.uk (S.P. Polisetty), b.pal@imperial.ac.uk (B.C. Pal).
[1] Student Member, IEEE
[2] Fellow, IEEE

https://doi.org/10.1016/j.epsr.2026.113579
Received 15 October 2025; Received in revised form 13 March 2026; Accepted 21 June 2026
Available online 30 June 2026
0378-7796/© 2026 The Author(s). Published by Elsevier B.V. This is an open access article under the CC BY license (http://creativecommons.org/licenses/by/4.0/).

Nomenclature

Notation

A_T	Incidence matrix of the thermal network.
B_E	Set of electrical network branches.
BFM	Branch Flow Model.
C&CG	Column-and-Constraint Generation.
CFVT	Constant Flow Variable Temperature.
DHS	District Heating System.
E_T	Set of all thermal network branches.
EV	Electric Vehicle.
FES	Flexible Energy Storage.
HWT	Hot Water Tank.
IES	Integrated Energy System.
IEHS	Integrated Electric–Heat System.
KKT	Karush–Kuhn–Tucker conditions.
N_E	Set of all electrical network nodes.
N_T	Set of all thermal load nodes.
RES	Renewable Energy Sources.
RO	Robust Optimization.
SAA	Sample Average Approximation.
SO	Stochastic Optimization.
SOC	State of Charge.
V2G	Vehicle-to-Grid.
η_{eb}	Efficiency of the electric boiler.

Parameters

α	Compensation cost for EV scheduling.
c_p	Specific heat capacity of water.
E_i^{batt}	Battery capacity of EV i.
$\dot{m}_p$	Vector of pipe mass flow rates.
$\dot{m}_q$	Vector of nodal net injections.
$\hat{p}^w$	Forecast output of the wind farm.
$p_{l,j}$	Real power demand at node j.
P_g	Power purchased from the substation.
$P_i^{\max}$	Maximum charging power of EV i.
p^w	Actual output of the wind farm.
π_t	Electricity price at time t.
y_i	Shunt admittance at node i.
z_{ij}	Impedance of line ij.

Variables

$\delta_{i,t}$	Scheduling variable of EV i at time t.
I_{ij}	Branch current flowing in line ij.
l_{ij}	Squared branch current magnitude in line ij.
$p_{ev,j}$	EV real power exchanged grid at node j.
p_j	Real power generated at node j.
$P_{i,t}^{ch}$	Grid-interactive power of EV i at time t.
P_{ij}	Real power flow in line ij.
p_g^w	Real power generated by renewable unit.
q_j	Reactive power generated at node j.
Q_{ij}	Reactive power flow in line ij.
S_{ij}	Complex power flow in line ij.
T_i	Temperature at node i of the heating network.
$T_{j,t}^{p+}$	Outflow temperature of the supply pipe.
$T_{j,t}^{p-}$	Inflow temperature of the supply pipe.
V_i	Voltage magnitude at node i.
v_i	Squared voltage magnitude at node i.

provides an alternative by optimizing against uncertainty sets without requiring full distributional information [10,11]. Recent studies have explored the integration of EVs and V2G technologies in multi-energy systems under uncertainty [12–14]. For example, Wang et al. [15] and [14] investigate EV participation in integrated energy systems mainly from a system planning perspective, where the objective is to determine the capacity configuration of system components rather than operational scheduling. Zhang et al. [16] focus on heuristic scheduling strategies for multi-energy virtual power plants. Robust optimization approaches have also been developed for multi-energy systems with EV participation [13,17]. However, these studies generally focus on system-level scheduling formulations, while the physical network constraints of coupled electrical and heating networks are not explicitly incorporated.

To incorporate network constraints in multi-energy scheduling, the modelling of electrical and heating networks requires a balance between physical fidelity and computational tractability. For district heating systems (DHS), the hydraulic and thermal dynamics are highly complex, and full-scale modelling often leads to excessive computational burden [18]. Therefore, simplified formulations such as the constant-flow variable-temperature (CFVT) model are widely adopted to capture the main thermal characteristics with improved computational efficiency [19–21]. For radial electrical distribution systems, the linearized power flow model LinDistFlow is also commonly used to represent network constraints with acceptable accuracy and tractability [22]. These models enable tractable representations of electricity and heating networks in optimization-based scheduling.

To address these gaps, the main contributions of this paper are summarized as follows:

- A network-constrained formulation explicitly couples the radial distribution system, district heating network, EV fleets with V2G capability, and electric boilers equipped with hot water tanks (HWTs), accurately representing both electrical and thermal operating limits.
- The two-stage robust scheduling with day-ahead EV scheduling decisions is built in this paper. A day-ahead decision layer determines EV charging/discharging schedules subject to user availability and travel constraints, while a second-stage recourse layer adaptively dispatches grid and thermal resources in response to realized renewable generation.
- To enable a structurally scalable robust optimization solution for the integrated energy system, a customized column-and-constraint generation (C&CG) algorithm is developed, which mitigates the scenario explosion associated with sample average approximation (SAA) through iterative cut generation while ensuring feasibility under network constraints and robustness against renewable uncertainty.
- Comparative studies with SO under uncertain renewable generation scenarios show that the proposed robust approach achieves lower worst-case operating cost while maintaining electrical and thermal network security.

The rest of this paper is organized as follows. Section 2 presents the modelling of the integrated electricity–heat system (IEHS), including the LinDistFlow-based power network, the mass and energy conservation-based district heating network, and the electric vehicle scheduling model under the V2G paradigm. Section 3 formulates the optimization problems, including the two-stage SO and the two-stage RO, and discusses their key technical challenges. Section 4 introduces the C&CG algorithm used to solve the RO problem. Section 5 provides case studies on an IEEE 15-bus distribution network coupled with a 5-node district heating system, comparing the performance of SO and RO under worst-case wind generation scenarios and analyzing cost, flexibility utilization, and computational performance. Section 6 concludes the paper and outlines potential future research directions.

2. Mathematical modelling

In this section, the mathematical modelling of the heat–power–V2G coupled system is presented. The system consists of a distribution network and a DHS. The distribution network includes a substation, distributed wind generation, parking lots with V2G-enabled EVs, fixed electrical loads obtained from day-ahead forecasts using historical day-ahead load profiles, and electric boilers as heat–power coupling devices.

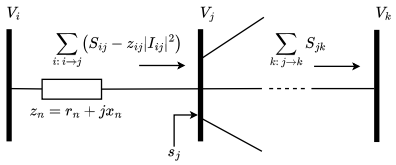


Fig. 1. BFM in a distribution system.

Electric vehicles are connected to the distribution network through charging facilities and can act as both flexible loads and storage units. The DHS consists of conventional boilers and electric boilers. In the proposed model, the conventional boiler is represented in a simplified manner using a fixed fuel cost coefficient, without considering detailed fuel properties, boiler technology characteristics, or unit-level operational dynamics. The electric boilers are equipped with hot water storage tanks as thermal storage units and serve as heat–power coupling elements between the power and heating systems.

2.1. Electrical power system modelling

Fig. 1 illustrates the branch flow model (BFM) [23] centered at bus j, together with its upstream bus i and downstream buses k.

The branch voltage drop equation can be written as,

$$V_i - V_j = z_{ij} I_{ij}, \quad \forall (i,j) \in B_E \tag{1}$$

Here, V_i and V_j denote the voltages at nodes i and j, respectively; I_{ij} is the current flowing from node i to node j; z_{ij} represents the branch impedance with resistance r_{ij} and reactance x_{ij}; and B_E denotes the set of electrical branches.

$$S_{ij} = V_i I_{ij}^*, \quad \forall (i,j) \in B_E \tag{2}$$

Based on (2), the power balance at each node j can be written as,

$$\sum_{k:\, j\to k} S_{jk} - \sum_{i:\, i\to j} \left(S_{ij} - z_{ij}|I_{ij}|^2\right) + y_j^* |V_j|^2 = s_j \tag{3}$$

Here, the notation $j \to k$ represents the branch from the upstream node j connected to downstream node k; and S_{ij} is complex power flow in line ij. By substituting the definitions

$$v_j := |V_j|^2, \quad l_{ij} := |I_{ij}|^2 \tag{4}$$

into (1)–(3), the DistFlow equations are obtained, which provide a real-valued representation of distribution networks. The complex power flows are separated into their real and imaginary parts, leading to (5)–(8).

$$p_j = \sum_{k:\, j\to k} P_{jk} - \sum_{i:\, i\to j} \left(P_{ij} - r_{ij} l_{ij}\right), \forall i,j \in N_E \tag{5}$$

$$q_j = \sum_{k:\, j\to k} Q_{jk} - \sum_{i:\, i\to j} \left(Q_{ij} - x_{ij} l_{ij}\right), \forall i,j \in N_E \tag{6}$$

$$v_i - v_j = 2\left(r_{ij} P_{ij} + x_{ij} Q_{ij}\right) - \left(r_{ij}^2 + x_{ij}^2\right) l_{ij}, \forall (i,j) \in B_E \tag{7}$$

$$v_i\, l_{ij} = P_{ij}^2 + Q_{ij}^2, \forall (i,j) \in B_E \tag{8}$$

Here, N_E denotes the set of all electrical network nodes, and P_{ij} and Q_{ij} represent the real and reactive power flows in line ij. The branch flow Eqs. (5)–(8) are non-convex and non-linear due to the quadratic terms in branch currents and power flows. When the network does not include voltage regulation devices and the research objective does not involve reactive power optimization, neglecting the quadratic loss terms provides a reasonable approximation [22]. Under these conditions, the LinDistFlow model (9)–(11) is widely used as a linearized representation of distribution networks [24].

$$\sum_{k:\, j\to k} P_{jk} = P_{ij} + p_j, \forall i,j \in N_E \tag{9}$$

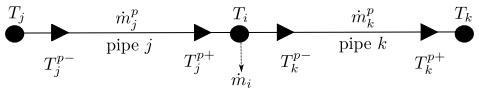


Fig. 2. Pipes representation in district heating system [21].

$$\sum_{k:\, j\to k} Q_{jk} = Q_{ij} + q_j, \forall i,j \in N_E \tag{10}$$

$$v_i - v_j = 2\left(r_{ij} P_{ij} + x_{ij} Q_{ij}\right), \forall (i,j) \in B_E \tag{11}$$

The net active power consumption p_j at each bus is formulated according to the connected devices: for RES buses, $p_j = p_{l,j} - p_g^w$; for substation buses, $p_j = p_{l,j} - P_g$; for EV buses, $p_j = p_{l,j} - p_{ev,j}$; and for buses with electric boilers, $p_j = p_{l,j} + p_{eb,j}$.

2.2. Electric vehicle V2G modelling

To model the charging–discharging flexibility of EVs, we define $P_{i,t}^{ch}$ as the grid-interactive power of EV i at time t, positive for charging and negative for discharging. Aggregator schedules EVs in the first stage to satisfy the grid requirement and final state of charge (SOC) requirement. A binary charging–discharging indicator $\delta_{i,t} \in \{0,1\}$ is introduced:

$$-P_i^{\max} \delta_{i,t} \le P_{i,t}^{ch} \le P_i^{\max} (1 - \delta_{i,t}) \tag{12}$$

$$\mathrm{SOC}_{i,t+1} = \mathrm{SOC}_{i,t} + \frac{P_{i,t}^{ch}\, \Delta t}{E_i^{batt}} \tag{13}$$

where $P_i^{\max}$ denotes the maximum exchange power capacity of EV i with the grid, which is taken symmetric for charging and discharging in this paper.

Eq. (14) specifies the initial SOC of the i-th vehicle battery at the beginning of each day, where $\mathrm{SOC}i^{init}$ represents EVs' initial SOC level. Eq. (15) ensures that the terminal SOC meets the target requirement, where $\mathrm{SOC}i^{final}$ denotes the desired final SOC level of vehicle i to guarantee sufficient reserved energy.

$$\mathrm{SOC}_{i,1} = \mathrm{SOC}_i^{init} \tag{14}$$

$$\mathrm{SOC}_{i,T} \ge \mathrm{SOC}_i^{final} \tag{15}$$

2.3. District heating network modelling

We adopt a CFVT representation [19], in which mass–flow rates are fixed while temperatures evolve according to energy balances and pipe losses. Thus, the detailed hydraulic equations no longer need to be solved, while the essential thermal transport dynamics are still preserved. Fig. 2 illustrates the CFVT-based pipe representation in the district heating system.

Define $\dot{m}_p \in \mathbb{R}^{|E_T|}$ as the vector of pipe mass flows, and $\dot{m}_q \in \mathbb{R}^{|N_T|}$ as the vector of nodal net injections, where a positive sign indicates supply and a negative sign indicates demand. Under CFVT the time–varying mass balance is linear:

$$\dot{m}_q = A_T\, \dot{m}_p \tag{16}$$

We assume a radial topology so that (16) yields a unique flow solution.

Let c_p be the specific heat capacity, T_a the ambient temperature, and N_T the set of heat nodes. For $\forall i,j \in N_T$, with incoming pipes $j \to i$ and outgoing pipes $i \to k$, the energy balances are given by,

$$\sum_{j:\, j\to i} c_p\, \dot{m}_{j,t}^p\, T_{j,t}^{p+} = \sum_{k:\, i\to k} c_p\, \dot{m}_{k,t}^p\, T_{k,t}^{p-} + c_p\, \dot{m}_{i,t}\, T_{i,t} \tag{17}$$

$$\sum_{j:\, j\to i} c_p\, \dot{m}_{j,t}^p\, T_{j,t}^{p+} + h_{s,i,t} = \sum_{k:\, i\to k} c_p\, \dot{m}_{k,t}^p\, T_{k,t}^{p-} + c_p\, \dot{m}_{i,t}\, T_a \tag{18}$$

Eq. (17) describes the energy balance on user nodes and (18) describes the energy balance on conventional source nodes.

For a node i hosting an electric boiler and a HWT, the energy balance augments (17) as,

$$\sum_{j:\, j\to i} c_p\, \dot{m}^p_{j,t}\, T^{p+}_{j,t} + h_{eb,i,t} = \sum_{k:\, i\to k} c_p\, \dot{m}^p_{k,t}\, T^{p-}_{k,t} + c_p\, \dot{m}_{i,t}\, T_a + H^{HWT}_{i,t} \tag{19}$$

The HWT energy state and operational limits are:

$$E^{HWT}_{i,t+1} = E^{HWT}_{i,t} + H^{HWT}_{i,t}\,\Delta t \tag{20}$$

$$E_{\min} \le E^{HWT}_{i,t} \le E_{\max} \tag{21}$$

$$-H_{\max} \le H^{HWT}_{i,t} \le H_{\max} \tag{22}$$

where Δt represents the time step of the simulation. In this paper, a temporal resolution of 1 h is adopted.

In classical thermodynamics, the stored thermal energy is given by:

$$Q = mc_p\Delta T \tag{23}$$

Based on this relation, the maximum storage capacity can be derived as:

$$E_{\max} = \rho\, V\, c_p\, [\, T_{\max} - T_{\min}\,] \tag{24}$$

For each pipe $(j,i) \in E_T$ with overall loss coefficient λ_{ij} and length L_{ij}, the outlet temperature satisfies

$$T^{p+}_{ij,t} = \left(T^{p-}_{ij,t} - T_a\right) \exp\left(-\frac{\lambda_{ij}\, L_{ij}}{c_p\, \dot{m}^p_{ij,t}}\right) + T_a \tag{25}$$

Temperature continuity at nodes, source bounds, and nodal temperature limits are enforced as,

$$T_{i,t} = T^{p-}_{ij,t} \tag{26}$$

$$0 \le h_{s,i,t} \le h^{\max}_{s,i}, \qquad 0 \le h_{eb,i,t} \le h^{\max}_{eb,i} \tag{27}$$

$$T^{\min}_{node} \le T_{i,t} \le T^{\max}_{node} \tag{28}$$

The electric boiler establishes the coupling between the power and heat networks, following the relationship

$$p_{eb} = \eta_{eb}\, h_{eb} \tag{29}$$

where η_{eb} is the conversion efficiency.

2.4. Wind power generation model

The uncertainty of wind power output is modeled using an uncertainty set that contains all possible realizations. The bounds of this set are derived from the forecast standard deviation and Chebyshev's inequality [25]. Let p^w denote the actual output of a wind farm, and $\hat{p}^w$ denote its predicted output. The output is bounded by:

$$p^w_{\min} \;\le\; p^w \;\le\; p^w_{\max} \tag{30}$$

where $p^w_{\min}$ and $p^w_{\max}$ are the lower and upper bounds, respectively. Given the standard deviation of forecast error σ, Chebyshev's inequality ensures that

$$\Pr\left(\left|p^w - \hat{p}^w\right| \ge k\sigma\right) \le \frac{1}{k^2} \tag{31}$$

The notation $\Pr(\cdot)$ denotes the probability of an event, and (31) guarantees that the deviation exceeds $k\sigma$ occurs with a very small probability.

By choosing k, the bounds can be expressed as,

$$p^w_{\min} = \hat{p}^w - k\sigma, \quad p^w_{\max} = \hat{p}^w + k\sigma \tag{32}$$

Eq. (32) defines a box (interval) uncertainty set. Compared with more general polyhedral sets (e.g., convex-hull sets constructed from scenarios), the bounds in this work are directly calibrated from mean and variance information via Chebyshev's inequality. In contrast to budgeted uncertainty sets, which introduce an additional budget parameter to limit the extent of simultaneous deviations, the proposed formulation characterizes the deviation range through a single parameter k.

3. Optimization problem formulation

In this study, EVs and HWTs are modeled as flexible loads with adjustable energy capacity and power modulation, enabling them to accommodate wind-generation uncertainty. A relatively complete recourse assumption is adopted: for any first-stage decision and any realized wind profile within the uncertainty set, the EV charging/discharging energy in the second stage can be adjusted to ensure feasibility that satisfies all system constraints. In this framework, the operating cost is evaluated under the worst-case wind realization. The proposed two-stage robust optimization framework minimizes the worst-case operational cost C under all possible realizations of uncertainty. The min–max–min problem is formulated as:

$$C = \min_{x\in\mathcal{X}}\; \alpha \sum_{i\in\mathcal{V}}\sum_{t=1}^{T} \delta_{i,t} + \max_{p^w\in\mathcal{U}}\; \min_{y\in\mathcal{Y}(x,p^w)} \sum_{t=1}^{T} \left(\pi_t P^g_t + c_s h^s_t\right), \tag{33}$$

where x denotes the first-stage decision variables, including the EV scheduling variables $\delta_{i,t}$, which are determined before the wind power is realized. The uncertain wind generation p^w lies in the uncertainty set $\mathcal{U}$, modeled as a box-type uncertainty set. After p^w is realized, the second-stage recourse decisions y are adjusted to satisfy all system constraints and minimize the operating cost, where P^g_t and h^s_t denote the grid power purchase and heat supply, respectively. Moreover, α is the compensation cost coefficient for EV scheduling, π_t is the electricity price at time period t, and c_s is the fuel price of the heating subsystem.

Following the Benders-type decomposition, the two-stage robust optimization can be separated into a master problem (MP) and a subproblem (SP).

$$MP: \quad \min_{x\in\mathcal{X}}\; \alpha \sum_{i\in\mathcal{V}}\sum_{t=1}^{T} \delta_{i,t} + \eta \tag{34}$$

$$\begin{aligned} SP: \quad & \max_{p^w\in\mathcal{U}}\; \min_{y\in\mathcal{Y}(x,p^w)} \sum_{t=1}^{T} \left(\pi_t P^g_t + c_s h^s_t\right) \\ s.t. \quad & (9)-(11), \\ & (12)-(15), \\ & (17)-(22),\ (25)-(30). \end{aligned} \tag{35}$$

The master problem determines the first-stage variables and evaluates the worst-case second-stage cost via the auxiliary variable η, while the subproblem characterizes the recourse feasibility and cost under uncertainty u. This decomposition enables tractable solution of the overall robust optimization model.

Fig. 3 illustrates the proposed two-stage robust scheduling framework for the integrated electricity-heat system. In this framework, Stage 1 solves the master problem to determine the EV scheduling decisions, whereas Stage 2 solves the subproblem to identify the worst-case wind scenario and obtain the corresponding power and heat dispatch. The physical coupling between the electricity and heat systems is realized through the electric boiler.

4. Column-and-constraint generation algorithm for solving the two-stage RO

To solve the two-stage robust optimization model formulated in Section 3, we adopt a column-and-constraint generation (C&CG) algorithm. This iterative approach alternates between solving MP and SP, progressively refining the uncertainty set realizations and feasibility cuts until convergence. The overall C&CG procedure is illustrated in Fig. 4 for clarity.

In Algorithm 1, $f_1(x)$ corresponds to the first-stage objective in (34), $f_2(y)$ corresponds to the second-stage objective in (35), while $f_{\text{constraints}}(x,y,u)$ denotes the set of second-stage constraints in (35). The oracle step is implemented using a single-level reformulation based on

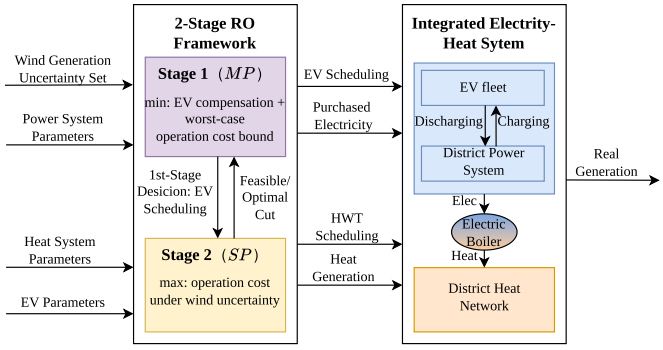


Fig. 3. Framework of the proposed two-stage robust scheduling for the integrated electricity–heat system.

Algorithm 1 Column-and-constraint generation.

Init: $LB \leftarrow -\infty$, $UB \leftarrow +\infty$, $k \leftarrow 0$, $\mathcal{O} \leftarrow \emptyset$
while $UB - LB > \epsilon$ **do**
  Solve master problem MP_k:
  $\min_{x\in\mathcal{X},\,\eta} f_1(x)+\eta$, *s.t.* optimality and feasibility cuts from $k-1$ step.
  Obtain $(x^*_{k+1}, \eta^*_{k+1})$ and set $LB \leftarrow f_1(x^*_{k+1}) + \eta^*_{k+1}$.
  Oracle: solve subproblem $\mathrm{SP}(x^*_{k+1})$
  $\mathcal{Q}(x^*_{k+1}) = \max_{u\in\mathcal{U}} \min_{y\in\mathcal{Y}} \{\, f_2(y) \mid s.t.\ f_{constraints}(x^*_{k+1}) \,\}$
  Update $UB \leftarrow \min\{\, UB,\ f_1(x^*_{k+1}) + \mathcal{Q}(x^*_{k+1}) \,\}$
  if $UB - LB \le \epsilon$ **then**

    return x^*_{k+1}
  else if $\mathcal{Q}(x^*_{k+1}) < +\infty$ **then**
    Let u^*_{k+1} be the oracle scenario and y^*_{k+1} its inner solution
    Add *optimality cut* $\eta \ge f_2(y^*_{k+1})$ and $f_{constraints}(u^*_{k+1}, y^*_{k+1})$
    $k \leftarrow k+1$
  else
    Identify a violating scenario u^{viol}_{k+1} and add *feasibility cut* $f_2(u^{viol}_{k+1})$ to MP_{k+1}
    $k \leftarrow k+1$
  end if
end while

the Karush–Kuhn–Tucker (KKT) conditions, where the inner minimization in SP is replaced by its corresponding KKT optimality system. These conditions are linearized into a set of mixed-integer constraints, thereby transforming the bilevel SP into a tractable MIP problem that can be solved by standard optimization software. The algorithm terminates when the optimality gap $UB - LB$ is less than a predefined tolerance ϵ, ensuring finite-step convergence.

5. Case study

The test platform consists of an IEEE 15-bus radial distribution network and a 5-bus district heating system. The IEEE 15-bus system as shown in Fig. 5a is modified to integrate RES and electric boilers. A RES unit is connected at Buses 11, and an EV parking area is connected at Bus 3. The 5-bus district heating system (see Fig. 5b) includes one electric boiler and a hot water tank connected at Bus 4, as well as a conventional heat source at Bus 1.

Key simulation parameters are listed in Table 1.

For the network shown in Fig. 5b, the node–pipe incidence matrix is given by

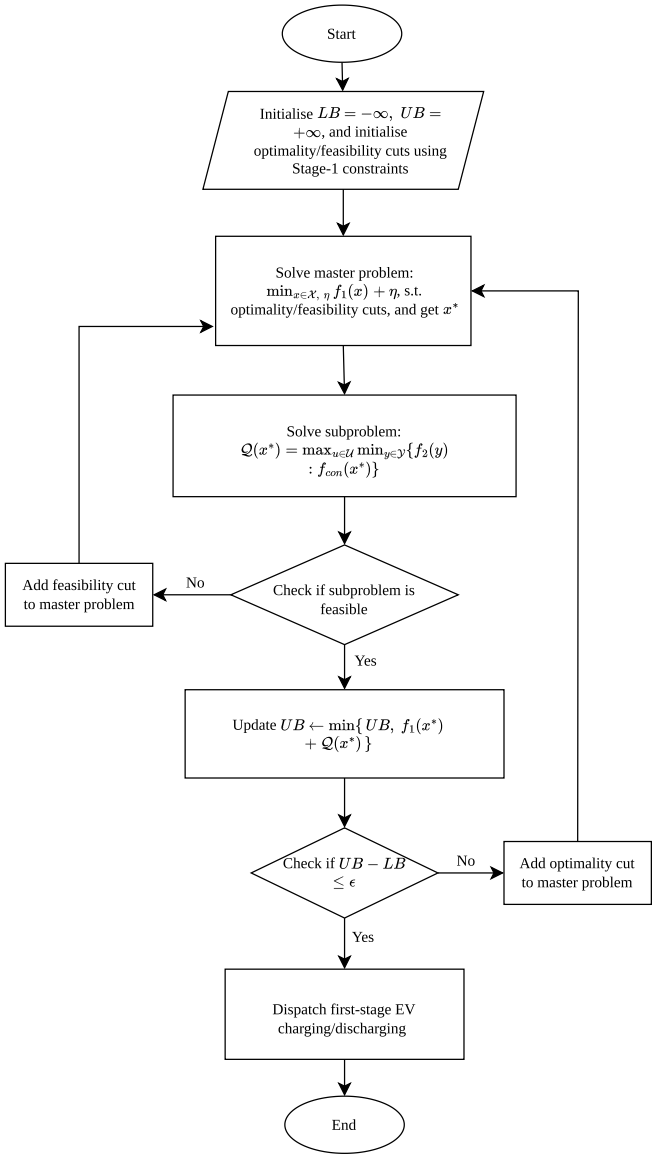


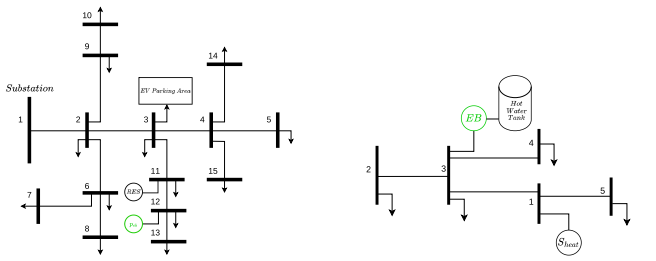
Fig. 4. Flowchart of two-stage robust optimisation framework.

Table 1
Simulation parameters.

Parameter	Value	Parameter	Value
$P_{eb,min}$	0 MW	$P_{eb,max}$	6 MW
$P_{g,min}$	0 MW	$P_{g,max}$	8 MW
$E^{HWT}_{\min}$	0 MWth	$E^{HWT}_{\max}$	5.815 MWth
$H^{HWT}_{\min}$	0 MW	$H^{HWT}_{\max}$	5 MW
λ	0.2	l_{pipe}	400 m
α	1 £/on-hour		

$$A_T = \begin{bmatrix} -1 & 0 & 0 & -1 \\ 0 & 1 & 0 & 0 \\ 1 & -1 & -1 & 0 \\ 0 & 0 & 1 & 0 \\ 0 & 0 & 0 & 1 \end{bmatrix}, \tag{36}$$

where rows correspond to nodes and columns correspond to pipes; an entry of $+1$ indicates that the flow in the corresponding pipe enters the node, -1 indicates that it leaves the node, and 0 indicates that the pipe is not connected to the node.



(a) A 15-bus radial distribution network. (b) A 5-bus district heating system.

Fig. 5. System description.

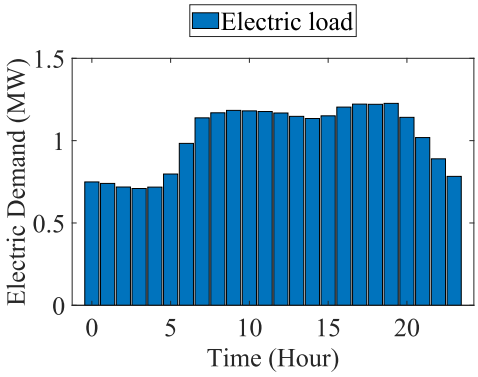


Fig. 6. Synthetic 24-h load profiles generated for the IEEE 15-bus system.

The load demand at each bus is time-varying and represented by a fixed 24-h load profile with a one-hour resolution. Since detailed bus-level load time series are usually not publicly available, the bus-level load $p_{j,t}$ is generated following the normalized peak-scaling approach proposed in [26], and the calculation is given by,

$$p_{j,t} = p_j^{\text{base}} \cdot p_t^{\text{norm}}, \quad p_t^{\text{norm}} = \frac{p_t}{\max p_t}, j \in N_E \tag{37}$$

where p_t denotes the system-level hourly load (MW) obtained from the Open Power System Data (OPSD) dataset [27], p_j^{base} denotes the nominal load (MW) at bus j, obtained from the MATPOWER IEEE 15-bus test system [28], and $p_t^{\text{norm}} \in [0, 1]$ is the normalized prototype profile. The resulting 24-h load profiles are shown in Fig. 6. Unlike the electrical load, the heat demand is not prescribed as a time-varying profile and is determined by the nodal mass flow rate, specific heat capacity, and nodal temperature.

5.1. Wind generation scenarios

The forecast wind generation data are taken as the mean input, while in the wind generation model (32), the standard deviation σ is set to 0.2 of the mean value with $k = 2$ to represent wind generation uncertainty. The resulting range of wind generation, illustrated in Fig. 7, corresponds to a box uncertainty set.

5.2. Two-stage stochastic approach

Within the wind generation range shown in Fig. 7, 100 Monte Carlo samples are drawn to capture wind uncertainty. The two-stage stochastic optimization aims to minimize the expected operating cost across these sampled scenarios. Following the sample average approximation (SAA) principle, the objective is formulated as,

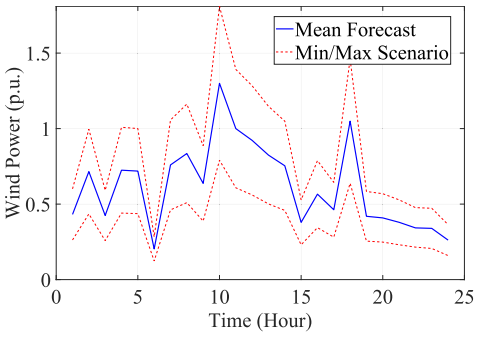
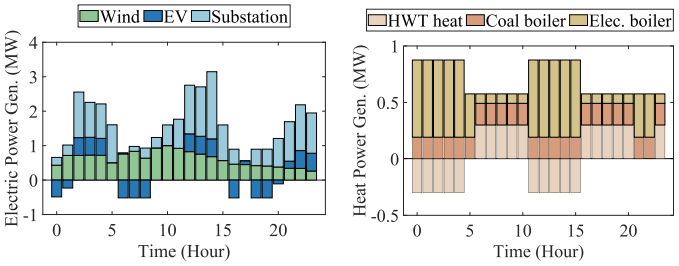


Fig. 7. Wind power scenarios with forecast uncertainty.



(a) Electrical power generated. (b) Heat power generated.

Fig. 8. Electric and heat power generation under the stochastic optimization scenario.

$$\min \frac{1}{N_s} \sum_{s=1}^{N_s} C^{(s)} \tag{38}$$

where N_s is the number of sampled scenarios and $C^{(s)}$ is the total operating cost under scenario s:

$$C^{(s)} = \alpha \sum_{i \in \mathcal{V}} \sum_{t=1}^{T} \delta_{i,t} + \sum_{t=1}^{T} \left(c_s h_s^{(s)}(t) + \pi_t P_g^{(s)}(t) \right) \tag{39}$$

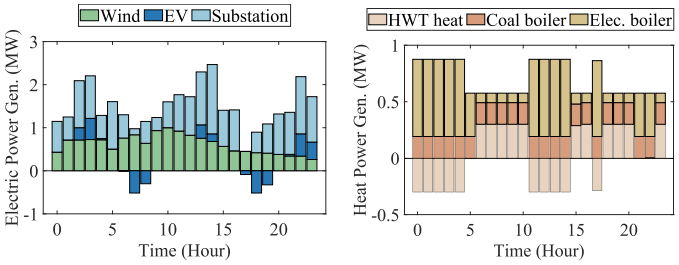
In (39), the operating cost includes the heat production cost $c_s h_s^{(s)}(t)$ and the electricity purchase cost $\pi_t P_g^{(s)}(t)$, where $h_s^{(s)}(t)$ and $P_g^{(s)}(t)$ are the scenario-dependent boiler heat output and substation imported power at time t under scenario s, respectively, and π_t is the day-ahead electricity price. The EV-related term $\alpha \sum_{i \in \mathcal{V}} \sum_{t=1}^{T} \delta_{i,t}$ is used to compensate the activation of first-stage EV discharging decisions. c_s, π_t, and α represent the heating fuel price, the electricity price at time period t, and the EV scheduling compensation cost, respectively; see Table 1 for their values, units, and data sources/assumptions.

After solving the SAA-based SO problem with 100 samples, the obtained first-stage decisions are evaluated under the identified worst-case wind scenario to assess cost robustness. Fig. 8a shows the resulting electrical power outputs from wind, EVs, and the substation under this scenario, while Fig. 8b presents the corresponding heat generation from the electric boiler, hot water tank, and conventional sources.

5.3. Two-stage robust approach

For the robust optimization, the wind generation uncertainty set is constructed as a box set with bounds defined by the forecast range in Fig. 7. C&CG algorithm iteratively identifies the worst-case wind trajectory, as shown in Fig. 10, and updates the master problem to ensure feasibility against all realizations within the uncertainty set.

The first-stage EV schedule generated by the RO model is then evaluated under the worst-case wind generation scenario, and the corresponding system operation is shown in Fig. 9.



(a) Electrical power generated (b) Heat power generated

Fig. 9. Electric and heat power generation under the robust optimization scenario.

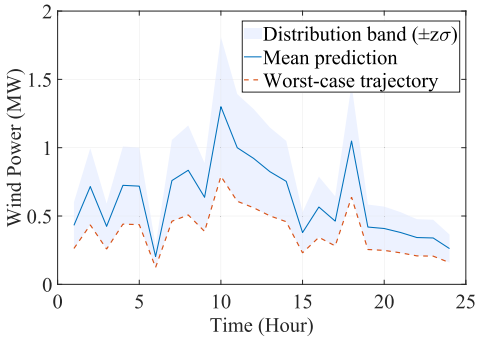


Fig. 10. Worst-case wind power trajectory identified by C&CG.

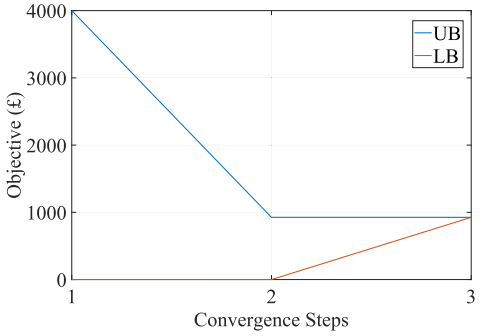


Fig. 11. Convergence of the C&CG algorithm (upper and lower bounds).

Compared to the dispatch results of the two-stage stochastic approach, the robust solution uses EV flexibility less intensively, leading to lower EV compensation costs, while the heat side shows reduced reliance on the HWT for thermal flexibility.

5.4. Comparison

5.4.1. Cost comparison between SO and RO

Table 2 shows the total operating costs of SO and RO under the worst-case wind power scenario identified by the C&CG algorithm, as illustrated in Fig. 10. Compared with SO, the total operating cost of RO is reduced by 27.2%, with costs of £925.619 and £1.150×10^3, respectively. The cost reduction occurs because SO tends to over-schedule EV discharging by assuming overly conservative wind outputs, leading to unnecessary compensation payments when the actual worst-case wind is less severe.

5.4.2. EV participation

Table 3 summarizes the total 24-h EV discharging energy. SO schedules more than twice the EV discharging compared with RO. This higher participation does not imply better utilization of EV flexibility, but rather excessive discharging caused by conservative wind assumptions, resulting in unnecessary transactions and higher costs. RO uses EV discharging only when necessary, maintaining feasibility with minimal cost.

Table 2
Operating cost comparison under different frameworks.

Cost Component	SO (£)	RO (£)
Heat Cost	10.553	10.553
Electricity Cost	924.174	757.086
EV Payment	215	158
Total Cost	1.150×10^3	925.619

Table 3
24-h EV discharging energy under different frameworks.

Framework	EV Discharging (MWh)
SO	3.933
RO	1.758

Table 4
Computational time comparison under different frameworks.

Method	Solver Time (s)
RO	319.62
SO	138.40

5.4.3. Computational performance

Table 4 reports the computational time of different optimisation methods. For the SAA-based SO, 100 sampled scenarios are used, leading to a solution time of about 138 s. Its computational burden increases rapidly with the number of scenarios because the second-stage variables and constraints grow significantly. For the proposed RO solved by the C&CG algorithm, the computational time is about 106 s per iteration. As shown in Fig. 11, the algorithm converges in three iterations, resulting in a total solution time of 319.6 s, as reported in Table 4. Moreover, unlike SAA, the proposed RO avoids scenario explosion while ensuring robustness. All simulations were running on an Intel Core i5-12500H processor with a maximum frequency of 4.5GHz.

From a computational perspective, the overall runtime is expected to increase for larger networks, as the dimensions of both the RO master problem and its adversarial subproblem grow with network size and the number of flexible resources. Moreover, stronger EV–network coupling and more conservative uncertainty modeling may require additional C&CG iterations to meet the convergence criterion, further increasing the computational effort.

6. Conclusion

In this paper, an optimization framework is developed for the joint scheduling of distribution power systems, district heating systems, and EVs under renewable generation uncertainty. The electrical distribution system is modeled using LinDistFlow equations and the thermal system is modeled using CFVT method. The proposed RO framework is solved using C&CG algorithm and SO framework is solved using SAA principle. The proposed formulation is validated on the IEEE 15-bus distribution network and a 5-node DHS. Compared with the SO approach, the RO method achieves more economical and resilient scheduling. While the SO approach with SAA is computationally efficient for a moderate sample size ($N = 100$), and it provides only an asymptotically unbiased estimate as $N \to \infty$. Whereas, with limited samples, the obtained solution may underestimate risk. The results confirm that flexibility resources such as HWTs and V2G-enabled EVs play a critical role in improving system feasibility and robustness. Improving computational efficiency for

large-scale instances will be considered in future work, including more efficient implementation and solver strategies for the iterative C&CG procedure.

CRediT authorship contribution statement

Muyang Li: Writing – original draft, Visualization, Validation, Software, Methodology, Formal analysis, Data curation, Conceptualization; **Sai Pavan Polisetty:** Writing – review & editing, Supervision, Methodology, Investigation, Formal analysis, Conceptualization; **Bikash C. Pal:** Writing – review & editing, Supervision, Project administration, Investigation.

Declaration of competing interest

The authors declare that they have no known competing financial interests or personal relationships that could have appeared to influence the work reported in this paper.

Data availability

We use open source data named Open Power System Data (OPSD) and cited it correctly.

References

[1] RenewableUK, Official stats show renewables generated over half of UK electricity for the first time in 2024, 2025. Accessed: Sep. 2025.
[2] L. Sani, Gone with the Wind? Grid Congestion and Wind Integration in GB, Technical Report, Carbon Tracker Initiative, 2023. Accessed: Sep. 30, 2025.
[3] X. Zhang, S.P. Jenne, Y. Ding, J. Spencer, W. He, J. Wang, A wind power curtailment mitigation strategy via co-location and co-operation of compressed air energy storage with wind power generation, Electr. Power Syst. Res. 241 (2025) 111318.
[4] G. De Carne, S.M. Maroufi, H. Beiranvand, V. De Angelis, S. D'Arco, V. Gevorgian, S. Waczowicz, B. Mather, M. Liserre, V. Hagenmeyer, The role of energy storage systems for a secure energy supply: a comprehensive review of system needs and technology solutions, Electr. Power Syst. Res. 236 (2024) 110963.
[5] R. Shi, S. Li, P. Zhang, K.Y. Lee, Integration of renewable energy sources and electric vehicles in V2G network with adjustable robust optimization, Renew. Energy 153 (2020) 1067–1080.
[6] International Energy Agency, Heating, 2022, [Online; accessed 30-May-2023].
[7] S.P. Polisetty, T. Joseph, A. Turk, E.I. Batzelis, B.C. Pal, G. Yang, P. Kotsampopoulos, Co-optimization of electrical and district heating networks: Bornholm case study, in: 2023 62nd IEEE Conference on Decision and Control (CDC), IEEE, 2023, pp. 2549–2554.
[8] C. Qin, Q. Yan, G. He, Integrated energy systems planning with electricity, heat and gas using particle swarm optimization, Energy 188 (2019) 116044.
[9] A. Rabiee, M. Sadeghi, J. Aghaeic, A. Heidari, Optimal operation of microgrids through simultaneous scheduling of electrical vehicles and responsive loads considering wind and PV units uncertainties, Renew. Sustain. Energy Rev. 57 (2016) 721–739.
[10] A. Ben-Tal, A. Nemirovski, L. El Ghaoui, Robust optimization (2009).
[11] R.A. Jabr, Adjustable robust OPF with renewable energy sources, IEEE Trans. Power Syst. 28 (4) (2013) 4742–4751.
[12] Q. Huang, Q.-S. Jia, X. Guan, Robust scheduling of EV charging load with uncertain wind power integration, IEEE Trans. Smart Grid 9 (2) (2016) 1043–1054.
[13] G. Wu, C. Yi, H. Xiao, Q. Wu, L. Zeng, Q. Yan, M. Zhang, Multi-objective optimization of integrated energy systems considering renewable energy uncertainty and electric vehicles, IEEE Trans. Smart Grid 14 (6) (2023) 4322–4332.
[14] H. Wei, Y. Zhang, Y. Wang, W. Hua, R. Jing, Y. Zhou, Planning integrated energy systems coupling V2G as a flexible storage, Energy 239 (2022) 122215.
[15] J. Wang, Y. Cui, Z. Liu, L. Zeng, C. Yue, Y.S. Agbodjan, Multi-energy complementary integrated energy system optimization with electric vehicle participation considering uncertainties, Energy 309 (2024) 133109.
[16] Z. Zhang, Y. Gao, Q. Ai, J. Yang, J. Zhao, J. Xiang, T. Lü, Multi-timescale energy management of multi-energy virtual power plant considering carbon trading mechanism and V2G interaction, in: 2025 IEEE Industry Applications Society Annual Meeting (IAS), IEEE, 2025, pp. 1–8.
[17] H. Xie, S. Gao, J. Zheng, X. Huang, A three-stage robust dispatch model considering the multi-uncertainties of electric vehicles and a multi-energy microgrid, Int. J. Electr. Power Energy Syst. 157 (2024) 109778.
[18] W. Tang, S. Huang, Load flow analysis of district heating systems by a newton-raphson method, in: 2019 IEEE 3rd Conference on Energy Internet and Energy System Integration (EI2), IEEE, 2019, pp. 1357–1362.
[19] X. Liu, J. Wu, N. Jenkins, A. Bagdanavicius, Combined analysis of electricity and heat networks, Appl. Energy 162 (2016) 1238–1250.
[20] N. Papakonstantinou, J. Savolainen, J. Koistinen, A. Aikala, V. Vyatkin, District heating temperature control algorithm based on short term weather forecast and consumption predictions, in: 2016 IEEE 21st International Conference on Emerging Technologies and Factory Automation (ETFA), IEEE, 2016, pp. 1–8.
[21] S.P. Polisetty, F.U. Nazir, B.C. Pal, Chance constrained co-optimization of integrated electrical and district heating networks, IEEE Trans. Power Syst. 40 (4) (2025) 3401–3412. https://doi.org/10.1109/TPWRS.2025.3527552
[22] M.E. Baran, F.F. Wu, Optimal capacitor placement on radial distribution systems, IEEE Trans. Power Del. 4 (1) (2002) 725–734.
[23] M. Farivar, S.H. Low, Branch flow model: relaxations and convexification-Part I, IEEE Trans. Power Syst. 28 (3) (2013) 2554–2564.
[24] L. Gan, S.H. Low, Convex relaxations and linear approximation for optimal power flow in multiphase radial networks, in: 2014 Power Systems Computation Conference, IEEE, 2014, pp. 1–9.
[25] W. Wei, F. Liu, S. Mei, Y. Hou, Robust energy and reserve dispatch under variable renewable generation, IEEE Trans. Smart Grid 6 (1) (2014) 369–380.
[26] H. Li, J.H. Yeo, A.L. Bornsheuer, T.J. Overbye, The creation and validation of load time series for synthetic electric power systems, IEEE Trans. Power Syst. 36 (2) (2020) 961–969.
[27] Open Power System Data, Data package time series, version 2020-10-06 (load, wind and solar, prices in hourly resolution), 2020, (Data set). https://doi.org/10.25832/time_series/2020-10-06
[28] D. Das, D.P. Kothari, A. Kalam, Simple and efficient method for load flow solution of radial distribution networks, Int. J. Electr. Power Energy Syst. 17 (5) (1995) 335–346.